MJFAS
Malaysian Journal of Fundamental and Applied Sciences

Ubaid *et al.* | Malaysian Journal of Fundamental and Applied Sciences, Vol. 22 (2026) 686-695

RESEARCH ARTICLE

# Precision Synthesis and Structural-Optical Characterization of Nickel Oxide Nanoparticles via Pulsed Laser Ablation in Liquid

**Ahmed Qasim Ubaid[a], Farzaneh Bayat[a*], Ali Aqeel Salim[b,c,**], Kazem Jamshidi-Ghaleha[a], Ali Reza Amani-Ghadim[d]**

[a]Physics Department, Faculty of Science, Azarbaijan Shahid Madani University (ASMU), Tabriz 53751-71379, Iran. [b]Physics Department & Laser Centre, Faculty of Science, Universiti Teknologi Malaysia (UTM), Johor, Malaysia. [c]Department of Laser and Optoelectronics Engineering, College of Engineering, University of Kut, Wasit, 52001, Iraq. [d]Applied Chemistry Research Laboratory, Department of Chemistry, Faculty of Basic Science, Azarbaijan Shahid Madani University (ASMU), Tabriz 53751-71379, Iran

Abstract. A sustainable ligand-free pulsed laser ablation in liquid (PLAL) strategy was used to synthesize nickel oxide nanoparticles (NiO-NPs) inside a chickpea extract liquid medium. A Nd:YAG pulsed laser was operated under constant laser parameters, including a wavelength of 1064 nm, pulse duration of 8 ns, and repetition rate of 8 Hz. The effect of laser fluences (LFs), ranging from 7.53 to 37.67 J/cm², on the structural, morphological, and optical characteristics of the synthesized NiO-NPs was determined. Transmission electron microscopy (TEM) and selected area electron diffraction (SAED) analyses revealed chemically stable, spherical NPs with an average diameter of ~11.6 ± 1.1 nm and polycrystalline structure. Ultraviolet-Visible (UV-Vis) spectroscopy exhibited a strong absorption band at ~261 nm with a bandgap ($E_g$) of ~4.15 eV. The slight reduction in $E_g$ with increasing LF was accompanied by enhanced band-edge absorbance and higher crystallinity, confirming the successful incorporation of bioactive capping compounds during laser-induced synthesis. Fluorescence spectra displayed a blue emission at ~450 nm with lifetime decay values increasing from 5.57 µs at the lowest LF of 7.53 J/cm² to 6.97 µs at higher LFs, indicating modified charge-carrier dynamics. The optimized NiO-NPs showed the scalability of chickpea phytochemical-assisted PLAL as a green and scalable route for creating multifunctional biofunctionalized metal oxide NPs. Thus, this work offers a sustainable and scalable route for developing high-performance, biofunctionalized NiO-NPs with tunable structural and optical properties suitable for next-generation optoelectronic applications.

**Keywords**: NiO-NPs; chickpea extract; laser ablation; structural; and optical properties.

## Introduction

A diverse array of nanoscale components, including carbon-based nanomaterials (CNMs), metal oxide nanoparticles (MNPs), and polymer nanocomposites (NCs) has been examined for the absorption, decomposition, and mineralization of persistent dye contaminants [1, 2]. MNPs/NCs have distinguished themselves as high-performance photocatalysts due to their tunable band-gap energies, exceptional surface reactivity, and structural adaptability, which offer superior light-harvesting, charge separation, and redox conversion efficiencies [3]. The strong optoelectronic properties of MNPs, including Au, Ag, Cu, $TiO_2$, ZnO, and NiO, have attracted significant attention for their ability to degrade persistent organic contaminants and destroy cell membranes [4-6]. Among these MNPs, nickel oxide (NiO) is distinguished as a flexible and sustainable photocatalyst due to its broad bandgap, low intrinsic toxicity, chemical durability, and multifunctional physicochemical properties across optical and electrical spectrums [7,8]. NiO-NPs have further been exploited in electrochemical storage systems, gas sensors, and transparent optoelectronics due to their defect-mediated charge transport and outstanding photostability [9]. Nonetheless, traditional methods for generating NiO-NPs like sol-gel, hydrothermal (HT), co-precipitation, and microwave-based approaches depend on hazardous precursors, multi-step processes,

***For correspondence:**
asali@utm.my

**Received:** 02 June 2026
**Accepted:** 22 June 2026

and high temperatures, which restrict scalability and compromise environmental sustainability [9,10]. Consequently, the development of green and sustainable synthesis strategies that integrate morphological precision, reproducibility, and ecological safety has emerged as a pivotal research frontier in modern NMs science [11].

Earlier, pulsed laser ablation in liquid (PLAL) had been demonstrated as a clean, cost-effective, and no-ligand technique for generating highly pure NPs with controllable geometries and composition [11-13]. This technique enables the exact adjustment of nanoparticle size and morphology through the utilization of customizable laser parameters, such as fluence, pulse duration, and repetition rate [14]. Incorporating PLAL with a bioactive or plant-derived medium offers an eco-friendly aspect by substituting synthetic stabilizers with organically sourced reduction agents [15]. In addition, NiO-NPs have exhibited significant antibacterial efficacy against gram-positive and gram-negative bacterial strains, broadening their utility in water treatment and purification technologies [16]. Khairnar et al. [17] developed NiO-NPs that could break down MB and rhodamine B, attaining a decomposition efficiency. These results confirmed the effectiveness of NiO-NPs, establishing them as viable multifunctional materials for sustainable optoelectronic applications.

Here, we provided an eco-friendly method for creating nickel oxide nanoparticles (NiO-NPs) using the PLAL. The bioactive constituents of the chickpea extract (e.g., polyphenols, proteins, and flavonoids) act as natural reducing and capping agents promoting the controlled nucleation, growth, and stabilization of NiO-NPs. The synthesized NiO-NPs were comprehensively characterized in terms of their optical absorption behavior, crystallographic structures, and nanoscale morphology. These findings demonstrated the synergistic role of laser fluence control, bioactive surface stabilization, and chemical structure. Thus, this work offers a sustainable and scalable route for developing high-performance NiO-NPs for optoelectronic applications. To the best of our knowledge, PLAL using chickpea extract for the green synthesis of NiO-NPs has not been previously reported.

# Materials and Methods

## Materials Used

A nickel metal target (99.9%, Sigma-Aldrich) was used for the ablation process. Pure ethanol (ET) and deionized water (DIW) were bought from Sigma-Aldrich. Fresh chickpeas (CP) were obtained from a local market in Iraq and promptly prepared to reduce oxidative destruction of compounds.

## Preparation of NiO-NPs

CP extracts were carefully cleaned with purified water to eliminate surface contaminants and immersed at ambient temperature (~25°C) for 24 hours to promote the extraction of aqueous-soluble phytochemicals [15]. To achieve a clear golden-brown liquid, the particles were homogenized using a high-frequency rotator. The resulting mixture was then simultaneously filtered using a Whatman No. 1 paper. A sustainable PLAL method with accurate ablation control was used to create NiO-NPs, as graphically illustrated in Figure 1. A cleaned Ni-based target was placed at the bottom of a glass cell containing 6 mL of newly extracted chickpea, being under magnetic rotation. A convex-plano lens with a focal length of 10 cm was used to focus a Q-switched Nd:YAG laser (wavelength of 1064 nm, pulse duration of 8 ns, and repetition rate of 8 Hz) onto the target surface. The laser fluence (LF) was adjusted from 7.53 J/cm² to 37.67 J/cm² to enhance the ablation efficiency, particle dimension, and morphological morphology. The duration of each ablation cycle was 20 minutes. The interaction between the laser beam and the target produced an intense plasma plume at the liquid-solid boundary. Fast quenching within short-term cavitation bubbles occurred when the high-temperature plasma released Ni ions, atoms, and clusters into the surrounding bioextract [18-20]. The physicochemical properties of the ablation medium significantly impacted crystallization, plasma confinement, and cooling dynamics, which eventually determined shell homogeneity. The combined effect between LF and the organic capping permitted fast oxidation and surface passivation, leading to uniformly distributed and defect-designed NiO-NPs with enhanced luminescence properties.

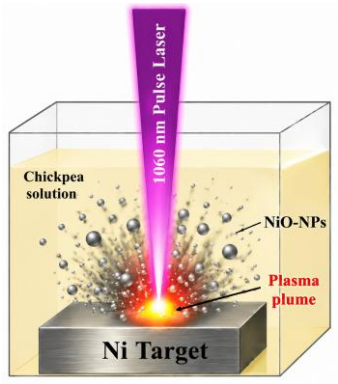


**Figure 1.** Schematic of the PLAL setup for the synthesis of NiO nanoparticles in chickpea extract.

### Characterization of NiO-NPs

The morphology of NiO-NPs was characterized using transmission electron microscopy (Hitachi HT7700) operated at an accelerating voltage of 120 kV. The optical properties of sample dispersions were analysed using a UV-Vis spectrophotometer (Shimadzu UV-3600 Plus) over the wavelength range of 200-800 nm, and the corresponding optical bandgap energy ($E_g$) was estimated using Tauc plot analysis. The pure chickpea liquid medium was used as the baseline/reference spectrum. Consequently, the intrinsic absorption of the extract was accounted for during spectral acquisition, and the resulting spectra predominantly reflect the optical characteristics of the synthesized NiO-NPs. Fluorescence properties, including CIE chromaticity coordinates and fluorescence lifetime decay, were investigated using a Fluoromax-4C and time-correlated single-photon counting (TCSPC) fluorescence (PTI QuantaMaster™ 60) spectrofluorometer at an excitation wavelength of 350 nm.

## Results and discussion

### Surface morphology

Figure 2 (a-d) exemplifies the TEM micrographs and SAED patterns of the synthesized NiO-NPs at an optimal LF of 30.14 J/cm². At high magnification, Figure 2b showed uniformly dispersed and spherical NiO-NPs decorated with chickpea organic shells. The average particle diameter (~11.6 ± 1.1 nm) was determined by measuring approximately 100 individual NPs from the TEM images using ImageJ software, indicating excellent control of nucleation and growth kinetics under the optimized laser parameters. The strong influence was evidenced by the chickpea-derived biomolecules in restricting secondary aggregation through surface complexation with $Ni^{2+}$species [21]. The higher-magnified image (Figure 2c) revealed the unique core-shell shape with a lighter amorphous layer formed from the CP organic-based material encircling a darker NiO crystal core. The layer derived from phytochemical constituents included amino acids, phenol compounds, and carbohydrate chains, which functioned as organic caps and reducing agents [15]. These moieties stabilized the high-energy NiO surface by interacting with the –OH, –COOH, and $–NH_2$ functionalities. This lowered the surface resistance and prevented particles from bonding together [22]. This bio-assisted encapsulation created a strong hybrid interface that made particles more stable and offered an active surface for charge transfer. The presence of distinct circular diffraction rings on the surface of NiO in the SAED pattern (Figure 2d) proved that the NiO cores were polycrystalline [23]. These outcomes revealed that highly crystallized NiO cores embedded within an organic shell made of CP biomolecules were generated using the eco-friendly PLAL approach.

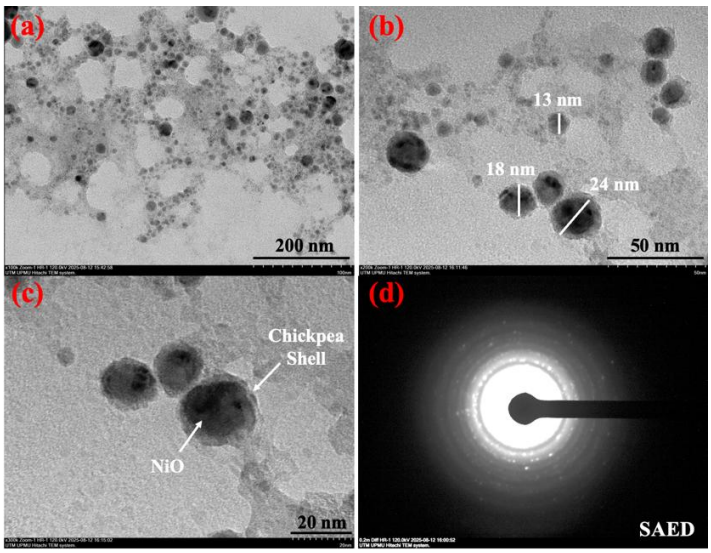


**Figure 2.** TEM images of the prepared NiO-NPs, (a) low-magnification overview, (b) particle morphology and size, (c) high-magnification core-shell structure, and (d) SAED patterns.

## Optical properties

Figure 3 shows the UV-Vis absorption bands of the synthesized NiO-NPs at varying LFs. It should be noted that the UV-Vis spectra were recorded relative to the solvent rather than to a pure chickpea extract reference; consequently, a minor contribution from the extract's intrinsic absorption cannot be entirely excluded. Future studies will include extract-only control spectra to isolate more precisely the optical response of the NiO-NPs. The absorption spectra exhibited two distinct optical regions, clarifying the evolution of NP formation, defect structure, and electronic transitions as a function of LF. The prominent absorption band appearing in the ~200–230 nm region corresponded to a combination of $\pi \rightarrow \pi$ and $\sigma \rightarrow \sigma$ transitions associated with organic molecules present in the chickpea extract (e.g., phenolic acids, flavonoids, and amino acids) that remain adsorbed onto the NiO surface [15]. These biomolecular moieties contributed to high-energy electronic transitions and acted as natural reducing and stabilizing agents, together enhancing photon capture efficiency and promoting homogeneous nucleation of NiO-NPs. The absorption bands allocated ~260–262 nm (inset) were attributed to Ni–O charge-transfer transitions and near-band-edge excitations within the NiO lattice [24]. This feature became progressively redshifted and more intense with increasing LFs (7.53–37.67 J/cm$^2$), indicating improved crystallinity, greater shell thickness, and a partial relaxation of the quantum confinement effect. The steady enhancement of absorption intensity indicated a higher population of optically active sites and a stronger electronic coupling between the NiO lattice and bio-organic capping species. In addition, the spectra revealed a gradual and broad absorption tail that arises from defect-mediated sub-band-gap states associated with oxygen vacancies ($V_o$), nickel interstitials ($Ni_i$), and surface disorder [25,26]. These defect levels acted as intermediate energy states that promoted photon absorption and facilitated charge carrier separation, which are beneficial for optoelectronic applications such as photodetectors and light-emitting devices.Thus, the spectral features confirmed that LF modulates the crystalline order, defect density, and optical response of the NiO-NPs.

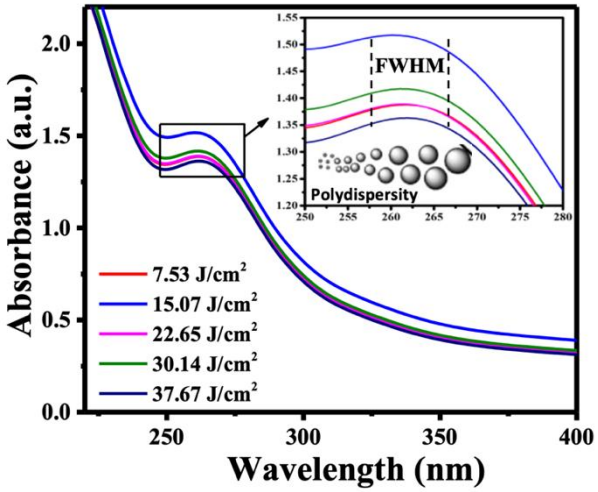


**Figure 3.** UV–Vis absorption spectra of NiO-NPs synthesized at different LFs (Insets (top right) show peak shift with increasing fluence)

Furthermore, the observed redshift and enhanced absorption intensity with increasing LF signify that higher ablation energies provide oxide formation and grain growth, causing a decrease in the optical energy bandgap ($E_g$) and improving photon-matter interactions. Effective optoelectronic performance depends on structurally adjustable NiO-NPs with improved light-harvesting features, which were achieved through the interaction of laser processing and biomolecular capping. The $E_g$ of the prepared NiO-NPs was determined using the Tauc relation [38].

$$(\alpha h\nu)^2 = A(h\nu - Eg) \quad (1)$$

where α denotes the absorption coefficient, hv represents the photon energy, and A is a proportionality constant. Figure 4 shows the plots of $(\alpha h\nu)^2$ versus hv. The direct $E_g$ values were obtained by extrapolating the linear portion of the curve to the photon energy axis.

The calculated optical $E_g$ values ranged from 4.15 to 4.19 eV, which are consistent with previously reported values of NiO-NPs [27]. The experimental uncertainty associated with the linear extrapolation of the Tauc plots was estimated to be approximately ±0.05 eV; accordingly, the small variation in $E_g$ observed across the different LFs (4.15–4.19 eV) indicates a relatively stable $E_g$ with only minor fluence-dependent modulation. As LF increased, there was a slight reduction in $E_g$, demonstrating improved crystallinity and quantum-confined effects. Furthermore, the optical transition energy may vary gradually due to the existence of interface-bound organic compounds and defect states, which could affect the electronic density of states within the conduction band. The tailoring in $E_g$ illustrated that LF was a significant factor for manipulating the electronic structure of NiO allowing the precise optimization of its optoelectronic and photocatalytic properties. $E_g$ increased band-edge absorbance and higher crystallinity, revealing the successful incorporation of bioactive capping compounds with laser-induced synthesis to produce superior NiO-NPs for UV wastewater treatment.

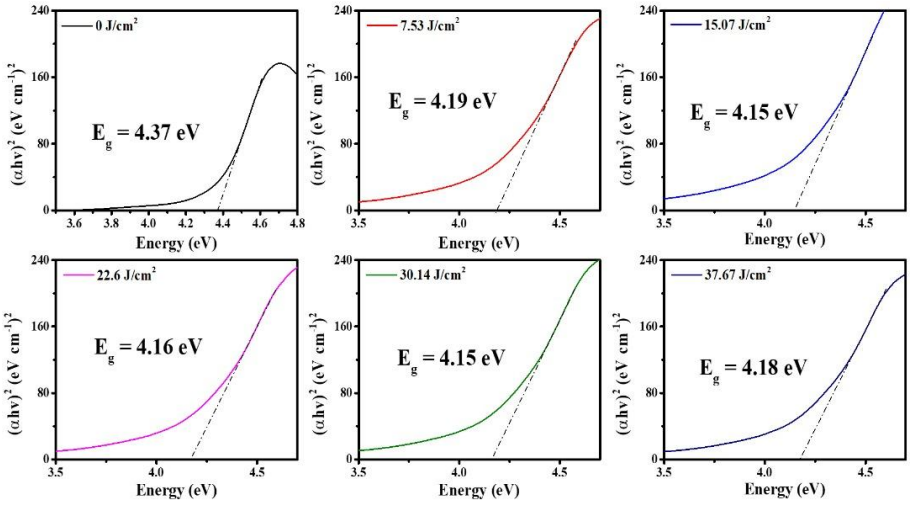


**Figure 4.** Tauc plots of $(\alpha h\nu)^2$ vs. photon energy for NiO-NPs at various LFs.

## Fluorescence features of NiO-NPs

Figure 5 displays the FL emission spectra of NiO-NPs synthesized in the chickpea extract medium under varying LFs. The spectra exhibited a prominent blue emission positioned at ~446 nm, affirming the existence of multiple electronic transitions in the NiO-NPs. The predominant emission was attributed to radiative recombination between defect-related $E_g$ levels and localised $Ni^{2+}/Ni^{3+}$states, which is characteristic of nonstoichiometric NiO and oxygen vacancies connected to the surface [26,27]. The emission intensity was found to be strongly dependent on LF; the untreated sample (0 J/cm$^2$) exhibited the highest FL intensity, which eventually decreases as fluence increases up to 37.67 J/cm$^2$. The gradual decrease in FL intensity signified fewer radiation-free recombination, attributable to increased crystalline structure and superior structural ordering at the higher LF. At lower fluences (≤15.07 J/cm$^2$), significant blue luminescence was produced due to a larger density of surface imperfections and oxygen shortages caused by incomplete oxidation. In contrast, increased fluences (≥22.65 J/cm$^2$) induced localised thermal annealing and defect elimination within the NiO lattice, lowering luminescence and enhancing charge carrier transport. The chickpea-derived biomolecules significantly contributed to defect modulation via acting as natural surfactants. interacting with surface Ni ions through –OH and –COOH groups and stopping too much charge from being trapped [28,29]. Interaction surface Ni ions through functional groups (such as –OH and –COOH) reduced excessive charge trapping, decreased shallow trap states, and enhanced electronic coupling between Ni and O orbitals [28]. Hence, the simultaneous effects of LF optimization and biomolecular stabilization refined the electronic structure of NiO, leading to more efficient charge separation, which is favorable for optoelectronic device performance.

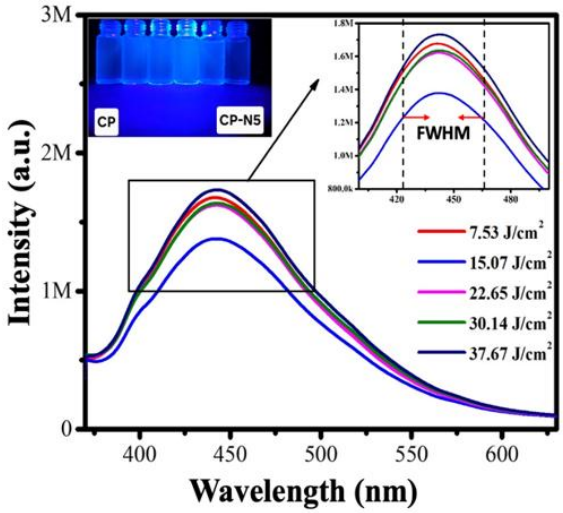

**Figure 5.** Fluorescence emission spectra of NiO-NPs at different LFs. Insets: (top-left) photographs of the samples under UV light; (top-right) FWHM of the emission peaks.

Figure 6 shows the time-resolved FL decay profiles of NiO-NPs to evaluate carrier recombination dynamics in the chickpea-assisted NiO-NPs. All samples exhibit bi-exponential decay behavior, indicative of two dominant recombination pathways: (i) (i) fast decay related to surface defect-mediated transitions and (ii) slow decay corresponding to bulk radiative recombination. The average FL lifetime (τ) for the CP alone was 6.24 µs, whereas the NiO-NPs synthesized at different LFs exhibited τ values between 5.57 and 6.97 µs. An increase in lifetime from 5.57 µs (7.53 J/cm$^2$) to 6.97 µs (37.67 J/cm$^2$) indicated a suppression of non-radiative recombination processes due to defect passivation and enhanced crystallinity at optimal fluence. The slight reduction in τ indicated the onset of localized heating and potential surface defect reformation at excessive fluences (>22.65 J/cm$^2$). The alterations in the lifetime were dependent on the charge carrier dynamics in NiO-NPs, those were influenced by customized LF. Optimized samples correlated with diminished FL intensity and displayed a longer lifetime, signifying enhanced charge separation and less recombination of photoinduced carriers. Due to their longer carrier lifetime, defect-mediated blue emission, and spectral stability, the bio-capped NiO-NPs were considered promising candidates for eco-friendly, luminescent nanomaterials for optoelectronic applications.

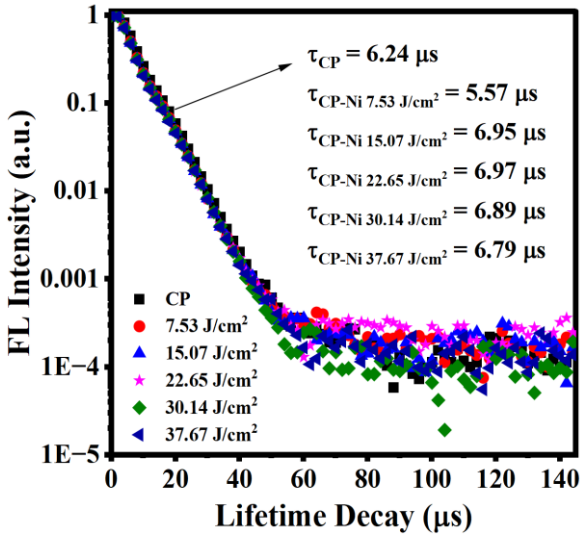


**Figure 6.** Time-resolved fluorescence decay and carrier lifetimes of NiO-NPs obtained at various LFs

## CIE Chromaticity coordinates

Figure 7 discloses the CIE chromaticity spectrum of NiO-NPs samples that were in the blue–cyan area. This confirmed blue emission is associated with electronic transitions where $Ni^{2+}$ changes to $Ni^{3+}$ [30]. A slight shift of the CIE coordinates was observed toward a greenish-blue spectrum with increased LF, indicating minor alterations in defect concentration and recombination mechanisms. The customization of this color further verified the impact of LF on the structure of the electronic bands and defect-associated optical changes of NiO-NPs. The relatively stable emission colour across all samples demonstrated that the CP bioextract successfully preserved electronic homogeneity despite laser-induced structural evolution.

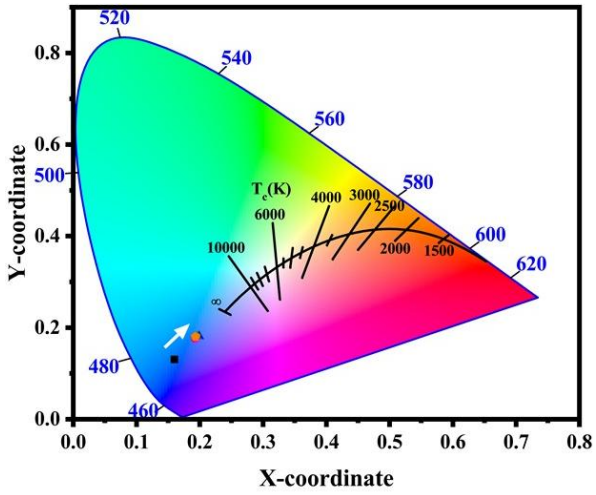


**Figure 7.** CIE 1931 chromaticity diagram with color temperature contours for NiO-NPs at various LFs.

**Table 1.** Optical characteristics of NiO-NPs as a function of laser fluences.

| Sample code | LFs ($J/cm^2$) | Absorption peak (nm) | $E_g$ (eV) | FL peak (nm) | FQY | CP (%) | CCT (K) | Lifetime decay (µs) |
|---|---|---|---|---|---|---|---|---|
| **CP-N1** | 7.53 | 260 | 4.19 | 442 | 0.037 | 53.53 | 7214 | 5.57 |
| **CP-N2** | 15.07 | 261 | 4.15 | 446 | 0.031 | 51.37 | 5854 | 6.94 |
| **CP-N3** | 22.65 | 262 | 4.16 | 444 | 0.038 | 53.28 | 6988 | 6.97 |
| **CP-N4** | 30.14 | 262 | 4.15 | 443 | 0.037 | 52.11 | 6360 | 6.89 |
| **CP-N5** | 37.67 | 262 | 4.18 | 445 | 0.04 | 52.61 | 3661 | 6.78 |

## Conclusion

The current research developed an economical and reproducible PLAL-based route for producing biofunctionalized NiO-NPs using chickpea extract as a natural stabilizing medium. The production provided exceptionally crystallized NiO encircled by a bio-organic outer layer, exhibiting a homogeneous shape, a smaller $E_g$ and modified electronic properties. The polycrystalline arrangements of NiO phase with an average size of ~11.6 ± 1.1 nm were verified by TEM and SAED analysis. The UV-Vis spectra showed a reduced $E_g$ of ~4.15 eV, demonstrating that the material was capable of absorbing better light. The fluorescence measurements exhibited a strong blue emission ~446 nm with the time-resolved decay durations ranging from 5.57 to 6.97 µs. Thus, the proposed green synthesis route provided an eco-friendly and cost-effective platform for producing biofunctionalized NiO-NPs with tunable structural and optical properties, making them promising candidates for future optoelectronic and photonic applications.

## Conflicts of Interest

The authors declare that there is no conflict of interest regarding the publication of this paper.

## Acknowledgment

This work has been financially supported by Azarbaijan Shahid Madani University under the grant number 1148/1404. Also, authors are thankful to RMC-UTM for financial support through the grant UTMFR Vot. No. 23H48 and 21H78.

## References


[1] Kumar, K. H., Ananda, H. T., Ravishankar, D. K., Madhu, H., & Thirumala, S. (2025). A review on nano metal oxides and their nanocomposites for photocatalytic degradation of dyes. Sustainable Chemistry One World, 100055.

[2] Niaz, U., Salim, A. A., Jamil, A., Salleh, M. S., Apsari, R., & Aziz, M. S. (2025). Optimized photocatalytic degradation of naproxen in aquatic environments using cerium oxide nanostructures: Morphological effects and laser-enhanced performance. *Materials Chemistry and Physics*, 131337.

[3] Al Miad, A., Saikat, S. P., Alam, M. K., Hossain, M. S., Bahadur, N. M., & Ahmed, S. (2024). Metal oxide-based photocatalysts for the efficient degradation of organic pollutants for a sustainable environment: a review. Nanoscale Advances, 6(19), 4781-4803.

[4] Sahu, S. K., Palai, A., & Sahu, D. (2024). Photocatalytic applications of metal oxide-based nanocomposites for sustainable environmental remediation. Sustainable Chemistry for the Environment, 8, 100162.

[5] Alhajj, M., Abd Aziz, M. S., Huyop, F., Salim, A. A., Sharma, S., & Ghoshal, S. K. (2022). Prominent bactericidal characteristics of silver-copper nanocomposites produced via pulse laser ablation. *Biomaterials Advances*, *142*, 213136.

[6] Salim, A. A., Ghoshal, S. K., Krishnan, G., & Bakhtiar, H. (2020). Tailored fluorescence traits of pulse laser ablated Gold-Cinnamon nanocomposites. *Materials Letters*, *264*, 127335.

[7] Fite, M. C., Karse, S. D., & Gode, L. M. (2025). Optical and photocatalytic properties of nickel oxide nanoparticles. Journal of Crystal Growth, 660, 128163.

[8] Ravi, G., & Patra, N. (2025). Hydrothermally synthesized CuO/NiO composites as a promising photocatalyst for sunlight-driven organic pollutant degradation. Journal of Materials Science: Materials in Engineering, 20(1), 34.

[9] Atul, A. K., Srivastava, S. K., Gupta, A. K., & Srivastava, N. (2022). Synthesis and characterization of NiO nanoparticles by chemical co-precipitation method: an easy and cost-effective approach. Brazilian Journal of Physics, 52(1), 2.

[10] Obaida, M., Fathi, A. M., Moussa, I., & Afify, H. H. (2022). Characterization and electrochromic properties of NiO thin films prepared using a green aqueous solution by pulsed spray pyrolysis technique. Journal of Materials Research, 37(14), 2282-2292.

[11] Salim, A. A., Ghoshal, S. K., & Bakhtiar, H. (2021). Tailored morphology, absorption and bactericidal traits of cinnamon nanocrystallites made via PLAL method: Role of altering laser fluence and solvent. *Optik*, *226*, 165879.

[12] Yan, Z., & Chrisey, D. B. (2012). Pulsed laser ablation in liquid for micro-/nanostructure generation. Journal of Photochemistry and Photobiology C: Photochemistry Reviews, 13(3), 204-223.

[13] Alshammari, T. K., Ghoshal, S. K., Bakhtiar, H., Alhajj, M., Salim, A. A., & Alias, S. S. (2024). A deterministic mechanism for efficient removal of arsenic and lead from wastewater using rapidly synthesized TiO2-(α-Fe2O3) nanoshells. *Journal of Molecular Liquids*, *413*, 125958.

[14] Attallah, A. H., Abdulwahid, F. S., Ali, Y. A., & Haider, A. J. (2023). Effect of liquid and laser parameters on fabrication of nanoparticles via pulsed laser ablation in liquid with their applications: a review. *Plasmonics*, *18*(4), 1307-1323.

[15] Ubaid, A. Q., Salim, A. A., Bayat, F., Jamshidi-Ghaleha, K., & Amani-Ghadim, A. R. (2025). Laser-Engineered $SnO_2$ Nanoshells in Chickpea Phytomatrix: A Green Strategy for Efficient Photocatalytic Dye Degradation. *Topics in Catalysis*, 1-13.

[16] Moradnia, F., Fardood, S. T., Zarei, A., Heidarzadeh, S., & Ramazani, A. (2024). Green synthesis of nickel oxide nanoparticles using plant extracts: an overview of their antibacterial, catalytic, and photocatalytic efficiency in the degradation of organic pollutants. Iranian Journal of Catalysis, 14(1).

[17] Khairnar, S. D., & Shrivastava, V. S. (2019). Facile synthesis of nickel oxide nanoparticles for the degradation of Methylene blue and Rhodamine B dye: a comparative study. Journal of Taibah University for Science, 13(1), 1108-1118.

[18] Rahman, A., & Guisbiers, G. (2024). Synthesis of nickel-based nanoparticles by pulsed laser ablation in liquids: correlations between laser beam power, size distribution and cavitation bubble lifetime. Metals, 14(2), 224.

[19] Gondal, M. A., Saleh, T. A., & Drmosh, Q. A. (2012). Synthesis of nickel oxide nanoparticles using pulsed laser ablation in liquids and their optical characterization. Applied Surface Science, 258(18), 6982-6986.

[20] Salim, A. A., Bakhtiar, H., Bidin, N., & Ghoshal, S. K. (2018). Antibacterial activity of decahedral cinnamon nanoparticles prepared in honey using PLAL technique. *Materials Letters*, *232*, 183-186.

[21] Dikshit, P. K., Kumar, J., Das, A. K., Sadhu, S., Sharma, S., Singh, S., ... & Kim, B. S. (2021). Green synthesis of metallic nanoparticles: Applications and limitations. Catalysts, 11(8), 902.

[22] Mahdi Salih, A., Mohammed Ali Hassan, Z., Jasim Khamees, E., & Gençyılmaz, O. (2025). Physiological characteristics and green production NiO nanoparticle synthesis employing Moringa Oleifera lam extract to assess in vitro cytotoxicity, antibacterial. Scientific Reports, 15(1), 33869.

[23] Xu, C., Li, Y., Adams, R. A., Pol, V. G., Xiao, Y., Varma, A., & Chen, P. (2021). One-step combustion synthesis of carbon-coated NiO/Ni composites for lithium and sodium storage. Journal of Alloys and Compounds, 884, 160927.

[24] Suresh, L., Snega, R., Sravanthy, P. G., Saravanan, M., & MUTHUPANDIAN, S. (2024). Phytosynthesis of Nickel Oxide nanoparticles and their antioxidant and Antibacterial Efficacy studies. Cureus, 16(4).

[25] Verma, B., Kumar, A., Swart, H. C., & Kumar, V. (2025). Enhanced optical and electrical properties of NiO-GO composite thin films on flexible PET substrates for optoelectronic applications. Chemistry of Inorganic Materials, 5, 100097.

[26] Egbo, K. O., Liu, C. P., Ekuma, C. E., & Yu, K. M. (2020). Vacancy defects induced changes in the electronic and optical properties of NiO studied by spectroscopic ellipsometry and first-principles calculations. Journal of Applied Physics, 128(13).

[27] Bonomo, M. (2018). Synthesis and characterization of NiO nanostructures: a review. Journal of Nanoparticle Research, 20(8), 222.

[28] Firisa, S. G., Muleta, G. G., & Yimer, A. A. (2022). Synthesis of nickel oxide nanoparticles and copper-doped nickel oxide nanocomposites using phytolacca dodecandra l'herit leaf extract and evaluation of its antioxidant and photocatalytic activities. ACS omega, 7(49), 44720-44732.

[29] Aqeel Salim, A., Bidin, N., Bakhtiar, H., Krishna Ghoshal, S., Al Azawi, M., & Krishnan, G. (2018, May). Optical and structure characterization of cinnamon nanoparticles synthesized by pulse laser ablation in liquid (PLAL). In *Journal of Physics: Conference Series* (Vol. 1027, No. 1, p. 012002). IOP Publishing.

[30] Gandhi, A. C., & Wu, S. Y. (2017). Strong deep-level-emission photoluminescence in NiO nanoparticles. *Nanomaterials*, *7*(8), 231.